Extended x-ray-absorption fine-structure study of the local atomic structure in As^+ heavily implanted silicon

J. L. Allain, J. R. Regnard, and A. Bourret
Centre d'Etudes Nucléaires de Grenoble, DRFMC/SP2M/S, Boîte Postale No. 85X, 38041 Grenoble CEDEX, France

A. Parisini and A. Armigliato
Consiglio Nazionale delle Richerche, Istituto di Chimica e Tecnologia dei Materiali e Componenti per l'Elettronica, via de Castagnoli 1, 40126 Bologna, Italy

G. Tourillon
Laboratoire pour l'Utilisation du Rayonnement Electromagnétique, Batiment 209D, Université de Paris–Sud, 91405 Orsay, France

S. Pizzini
Department of Pure and Applied Chemistry, University of Strathclyde, Glasgow G1 1XL, Scotland
(Received 21 February 1991; revised manuscript received 28 April 1992)

Extended x-ray-absorption fine-structure (EXAFS) measurements were performed on As heavily implanted crystalline silicon, using total electron yield and fluorescence detection to study a large range of implanted doses: 5×10^{15}, 3, and 5×10^{16} As/cm^2. The electrical deactivation of these samples after laser and subsequent thermal annealing (from 350 °C up to 1000 °C) is studied through the evolution of the first two shells of neighbors around As atoms. For an annealing temperature lower than 750 °C, a model consistent with the EXAFS results is presented, in which the As deactivation is due to the formation of inactive clusters involving about 7 As atoms around one vacancy. For a higher annealing temperature (750–1000 °C) the EXAFS results suggest the coexistence of clusters and precipitates in equilibrium.

I. INTRODUCTION

Shallow junctions in crystalline silicon with high electrical conductivity, required by the microelectronics industry, are obtained by incorporating doping impurities such as As (or Sb, P, B) in excess of equilibrium limits using ion implantation. In case of n^+/p junctions, the most commonly used dopant is As. For heavy As implants the crystal regrowth of the amorphized layer can be effectively accomplished by liquid-phase epitaxy using pulsed-laser annealing. In this case, at an implantation energy of 100 keV, one can obtain a complete activation of the dopant up to a maximum dose of 4×10^{16} As/cm^2, a value far above the equilibrium carrier concentration. However, subsequent thermal annealing treatments, which are generally performed in the very large scale integrated technology, already at temperatures as low as 300 °C, result in a marked decrease of the carrier concentration toward the equilibrium value.[1–6]

Rutherford backscattering spectroscopy (RBS) measurements show that, after laser annealing, As atoms are substitutional, whereas a fraction of them are displaced from the Si lattice after subsequent thermal annealing.[3,7] Moreover, concomitantly to the deactivation phenomenon, extended defects, interstitial in nature, are formed.[2,8–10]

Many models have been proposed to explain the physical nature of the inactive dopant: the main ideas are the formation of precipitates[2,5,6,11] or of inactive clusters[7,12–17] in equilibrium with the As atoms in solution, or the coexistence of the two local structures.[1,11,18] The subject is still open, as the observed precipitates cannot explain all the inactive As atoms.[2] Moreover, the composition of these different structures is still unknown, even though many hypotheses have been proposed [small coherent, sphalerite type, SiAs precipitates,[2] As_3,[16] As_2V,[1,7,12] or As_4V (Ref. 13) clusters, associating several As atoms and, in some cases, a vacancy (V)]. Only recently, but for implantation doses higher than 1×10^{17} As/cm^2, large SiAs precipitates having the monoclinic structure previously reported by Wadsten[19] have been clearly identified by TEM experiments.[20] Also in this case, the total amount of As in the large SiAs precipitates represents only a fraction (about 15%) of the total inactive As concentration.

Pandey *et al.*[13] already applied the extended x-ray-absorption fine-structure (EXAFS) technique to this problem. They analyzed samples isochronally annealed for 30 min at annealing temperatures ranging from 200 °C up to 800 °C using only one very high implanted dose (6×10^{16} As/cm^2). They also presented a model of an inactive cluster (As_4V) which appears to be in agreement with their EXAFS results for an annealing temperature below 650 °C.

In a previous paper,[1] we reported electrical measurements, transmission electron microscopy, and double-crystal x-ray diffractometry performed on heavily implanted samples (from 1×10^{16} to 5×10^{16} As/cm^2) after laser and subsequent thermal annealing. We also proposed a model of the As deactivation that can be summarized as follows.

(i) At a given dose, low-temperature annealing gives

 ©1992 The American Physical Society

rise to As deactivation through the formation of an $(As_2V)^+$ cluster and a self-interstitial I^- as a first step of the deactivation process.

(ii) At higher temperatures, it was suggested that these clusters could agglomerate to form an As_mV cluster. These clusters could also be the embryos of the precipitates observed by electron microscopy.[2]

In this paper we present the results of EXAFS experiments performed on a larger range of implanted doses, i.e., 5×10^{15}, 1×10^{16}, 3×10^{16}, and 5×10^{16} As/cm^2, by using two different detection techniques: total electron yield (TEY) and fluorescence detection. We have focused our attention on two main problems: (i) the initial stage of the As deactivation phenomenon, and (ii) the evolution of these metastable alloys towards the equilibrium. The former point is investigated by an isothermal annealing at 350 °C at a dose of 3×10^{16} As/cm^2, while the latter is studied at higher annealing temperatures for doses ranging from 5×10^{15} to 5×10^{16} As/cm^2. From the evolution of the local order around an As atom, the different models of the As deactivation process previously proposed are discussed.

II. EXPERIMENT

A. Samples

{100} CZ *p*-type silicon wafers were implanted with arsenic at an energy of 100 keV and at doses of 5×10^{15} As/cm^2, 1×10^{16}, 3×10^{16}, and 5×10^{16} As/cm^2. This results in an amorphous layer about 150 nm thick as determined by electron microscopy on cross sections. Laser annealing was carried out with a Xe-Cl excimer laser in air with an energy density of 1.9 J/cm^2. A fast scanning of a square light spot of 16 mm^2 was used to cover the whole area of the samples. The highest As concentration that can be electrically activated after laser annealing is about 4×10^{16} As/cm^2. For As concentrations above this limit, some As atoms remain electrically inactive after laser annealing. This is the case for our samples implanted with a dose of 5×10^{16} As/cm^2 (see Table I) and most probably for the ones studied by Pandey *et al.*,[13] implanted with 6×10^{16} As/cm^2.

Subsequent thermal annealing was performed in N_2 atmosphere in a range of temperatures from 350 °C up to 1000 °C as shown in Table I. In this table, the electrical

TABLE I. Characteristics of the samples studied: the implanted dose, the annealing treatment (each thermal annealing was performed after a laser annealing), the electrical characteristics (C_{As^0} is the inactive As concentration, *f* is the fractional deactivation parameter defined in the text), the EXAFS detection mode, which was used on this sample (Fluo, fluorescence detection; TEY, total electron yield measurements).

Dose As^+/cm^2	Annealing Type	Annealing Time	Electrical characteristics $C_{As^0}(As^+/cm^2)$	*f*	EXAFS detection mode
5×10^{15}	Implanted				Fluo
	laser		0		Fluo
	650 °C	2 h	$\approx2.5\times10^{15}$	0.58	Fluo
	900 °C	30 min	$\approx2.5\times10^{15}$	1.00	Fluo
1×10^{16}	Laser		0		Fluo
3×10^{16}	Implanted				TEY
	Laser		0		Fluo,TEY
	350 °C	40 min	3.9×10^{15}	0.13	TEY
	350 °C	80 min	6×10^{15}	0.20	Fluo
	350 °C	640 min	1.6×10^{16}	0.55	TEY
	450 °C	4 h	$\approx2.7\times10^{16}$	0.90	Fluo,TEY
	550 °C	3 h	$\approx2.7\times10^{16}$	0.91	Fluo
	650 °C	2 h	$\approx2.7\times10^{16}$	0.94	TEY
	750 °C	1 h	$\approx2.8\times10^{16}$	0.99	TEY
	850 °C	30 min	$\approx2.7\times10^{16}$	1.00	TEY
	900 °C	30 min	$\approx2.7\times10^{16}$	1.00	TEY
	1000 °C	30 min	$\approx2.7\times10^{16}$	1.00	TEY
5×10^{16}	Implanted				TEY
	laser		1×10^{16}		TEY
	450 °C	4 h	$\approx4.6\times10^{16}$	0.92	TEY
	550 °C	3 h	$\approx4.7\times10^{16}$	0.95	TEY
	650 °C	2 h	$\approx4.7\times10^{16}$	0.96	TEY
	750 °C	1 h	$\approx4.7\times10^{16}$	0.98	TEY
	850 °C	30 min	$\approx4.7\times10^{16}$	0.99	TEY
	900 °C	30 min	$\approx4.7\times10^{16}$	1.00	TEY
	1000 °C	30 min	$\approx4.7\times10^{16}$	1.00	TEY

characteristics of these samples are reported as inactive As concentration C_{As^0} and fractional deactivation f. This latter parameter is given by

$$f=(C^{\mathrm{tot}}_{\mathrm{As}^+}-C_{\mathrm{As}^+})/(C^{\mathrm{tot}}_{\mathrm{As}^+}-C^{e}_{\mathrm{As}^+})\ ,$$

where $C^{\mathrm{tot}}_{\mathrm{As}^+}$, $C^{e}_{\mathrm{As}^+}$, and C_{As^+} are the initial, the equilibrium, and the measured carrier concentration, respectively. From a comparison of the values of C_{As^0} and f, it is worthwhile noting that for all doses employed, the equilibrium carrier concentration has been attained only at the highest annealing temperatures.

Several samples were used as model compounds for the EXAFS study: crystalline SiAs, amorphous arsenic, and crystalline GaAs [studied in total electron yield (TEY) detection] and a bulk-doped (BD) Si crystal with an As atomic concentration of 0.04% (studied in fluorescence detection).

B. EXAFS experiments

The As K-edge spectra of the model compounds and of most of the As-implanted samples (Table I) were carried out in a TEY detection mode. The experiments were performed on station EXAFS 1 at the storage ring DCI of Laboratoire pour l'Utilisation du Rayonnement Electromagnétique (LURE) using a Si{331} monochromator and a 2-mm vertical width for the entrance slit. The signal was recorded with the detector developed by Tourillon *et al.*[21] and the sample was positioned on a rotating sample holder to reduce the Bragg peaks. The electrons emitted from the rotating silicon wafers after the absorption process (photoelectrons, Auger electrons, and their secondary electrons) ionize the He atoms at atmospheric pressure. Low-energy electrons are collected by the aluminized mylar electrode polarized at +60 V. The contribution of an ejected electron is proportional to its kinetic energy as each He ionization requires 24.6 eV. The detector current is then dominated by the more energetic Auger electrons (9.1 keV). According to the formula given by Elam *et al.*,[22] the depth probed by this technique in the case of As in a Si matrix is about 4000 Å. Consequently, the whole implanted layer, about 1500 Å, is probed.

The As K-edge-fluorescence EXAFS measurements of the samples indicated as "Fluo" in Table I were performed at a grazing incidence angle on station 9.2 at Synchrotron Radiation Center, Daresbury Laboratory, using a monochromator Si{220} and a vertical width of the entrance slit of 0.4 mm. The harmonic rejection rate was kept constant to 50%. The fluorescence signal was monitored by a Canberra 13-element Ge solid-state detector, which has an energy resolution of about 100 eV at 10 keV. It allows the As fluorescence line to be selected for the recording of the EXAFS spectra and to eliminate the Bragg peaks, which appear in only some of the 13 detectors. The incidence angle of the x-ray beam on the sample was about 300 mdeg, about twice the critical angle for total external reflection at the As K edge.

For each sample, several spectra (from 3 to 6) were added to obtain a better signal-to-noise ratio. As an example, the absorption spectra of a 3×10^{16} As/cm^2 sample (after laser annealing), obtained by TEY and fluorescence detection, are shown in Fig. 1.

C. EXAFS analysis

For all samples and model compounds, data analysis was carried out using the same standard procedure: the oscillatory part of the x-ray absorption, normalized by the edge jump as proposed by Stöhr, Noguera, and Kendelwicz,[23] was isolated using a fourth-order polynomial expression. The EXAFS spectra of a 3×10^{16} As/cm^2 sample (after a laser annealing), measured by TEY and fluorescence detection, are shown in Fig. 2. Data are then Fourier transformed using a k^3 weighting and a window extending from 50 to 400 eV. The Fourier transforms (FT's) of some samples, obtained as described above, are reported in Figs. 3–5. As usual, the reported distances in these figures must be corrected to account

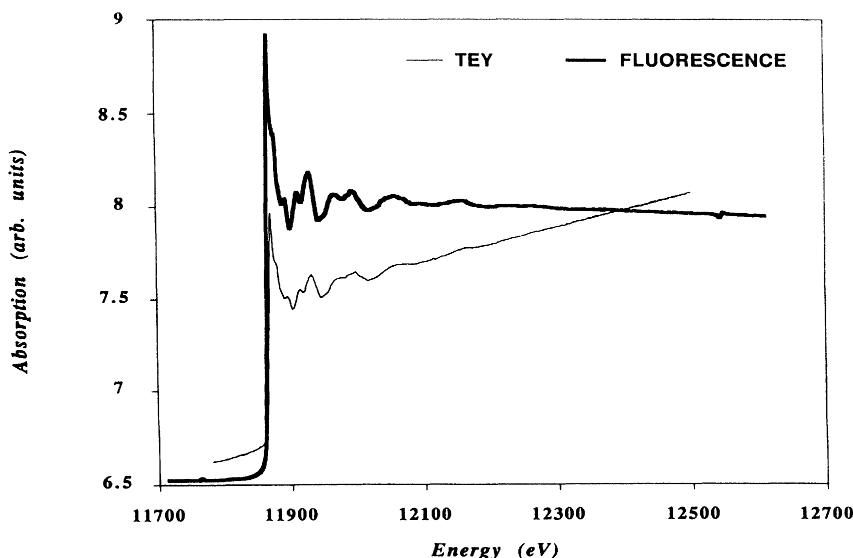

FIG. 1. Absorption spectra of a 3×10^{16}-As/cm^2 sample, after laser annealing, obtained by fluorescence and TEY detection. For comparison, the spectrum recorded by electron detection has been rescaled in amplitude.

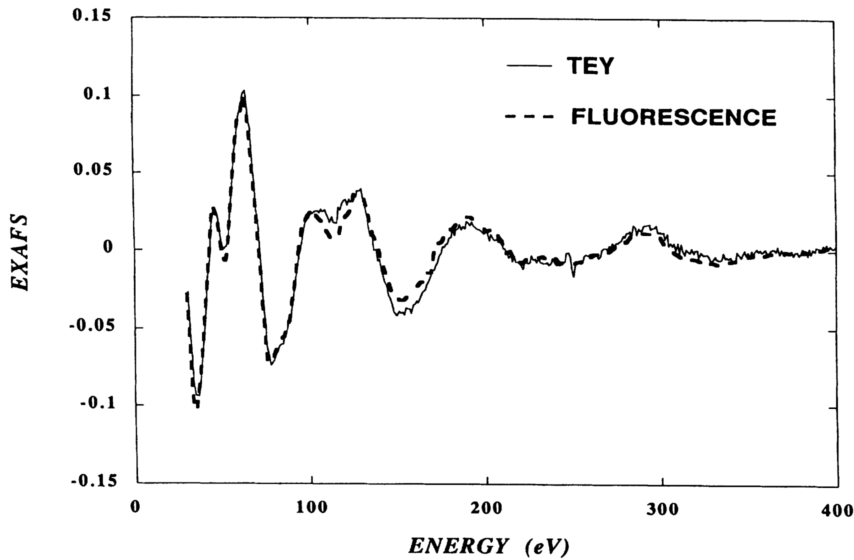

FIG. 2. EXAFS spectra of a 3×10^{16}-As/cm^2 sample, after laser annealing, obtained by fluorescence and TEY detection.

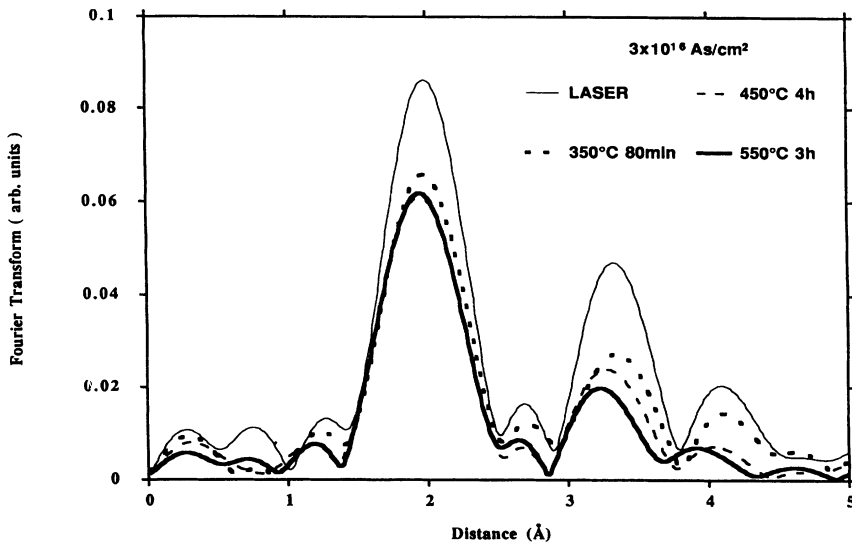

FIG. 3. Moduli of the Fourier transforms of several 3×10^{16}-As/cm^2 samples after laser annealing, after a subsequent annealing at 350 °C for 80 min, at 450 °C for 4 h, and 550 °C for 3 h. The EXAFS spectra were obtained by fluorescence detection at grazing incidence angle.

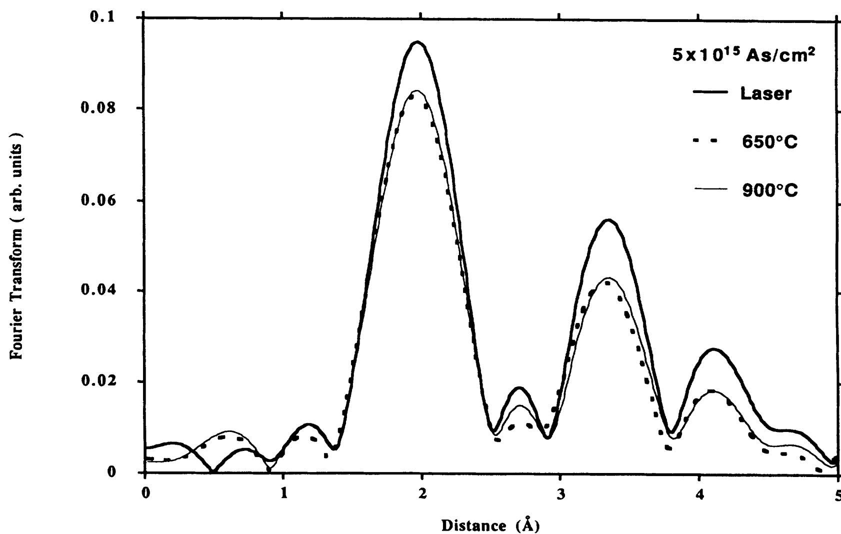

FIG. 4. Moduli of the Fourier transforms of several 5×10^{15}-As/cm^2 samples after laser annealing, after a subsequent annealing at 650 °C for 2 h, and at 900 °C for 30 min. The EXAFS spectra were obtained by fluorescence detection.

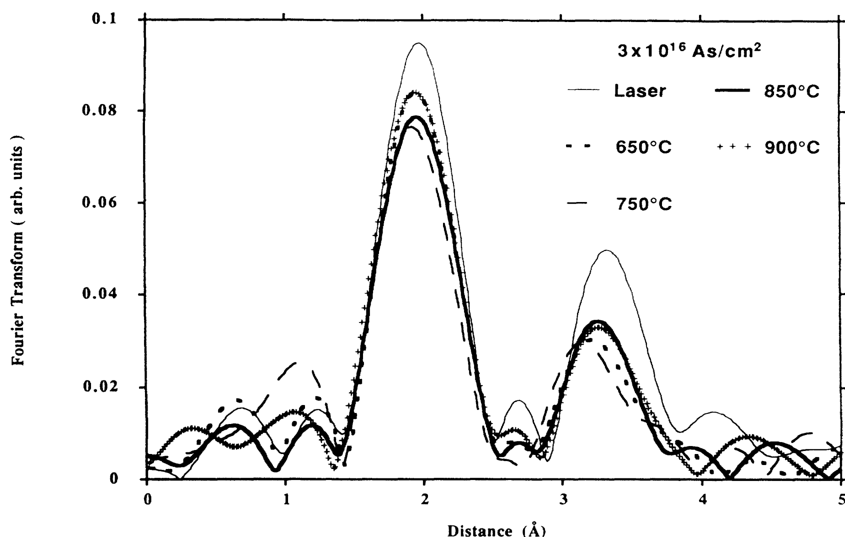

FIG. 5. Moduli of the Fourier transforms of several 3×10^{16}-As/cm^2 samples after laser annealing, after a subsequent annealing at 650 °C for 2 h, 750 °C for 1 h, 850 °C for 30 min, and 900 °C for 30 min. The EXAFS spectra were obtained by TEY.

for central and backscattered atomic phase shifts before obtaining the real distances reported in Table III. It is also worth noting that the magnitude of a peak of a FT is, for an ideal experiment, roughly proportional to N/σ where N is the number of atoms in the shell and σ the Debye-Waller factor (standard deviation of the distribution of distances). Therefore, the amplitudes of the different peaks are not proportional to the number of atoms, as the Debye-Waller factor was found to vary from one sample to another (see below).

An inverse Fourier transform of the first two peaks between 1.5 and 4.5 Å is then performed. The obtained data were analyzed using the least-square-fitting routine EXCURV88, based on curve-wave theory.[24] This program minimizes the parameter FI defined by

$$\mathrm{FI}=\frac{1}{N_{\mathrm{pts}}\times 100}\sum_{i}^{N_{\mathrm{pts}}}(\mathrm{data}_i-\mathrm{model}_i)^2k_i^3\ ,$$

where N_{pts} is the total number of points in the analyzed spectrum, data_i and model_i the experimental and theoretical values of the EXAFS signal at the wave vector k_i. The central atom (As) and backscattered phase shifts (As, Si) were calculated *ab initio* and refined using a linear correction. The choice of the model compound used to refine the theoretical phases is of importance and in Sec. II D we compare the results obtained with the SiAs and BD crystals as reference. An example of least-square-fitted data is shown in Fig. 6.

In order to appreciate the error bars on the fitted parameters and their correlations we have plotted the fitting-index contours corresponding to different values of the parameter FI defined above. The error bars associated with each parameter were obtained from the contour corresponding to the parameter FI equal to 1. It corresponds roughly to the value of FI calculated with the values of the parameters obtained by a fit on another spectrum of the same sample but measured during another experiment. Thus, it reflects the uncertainty of the experiment and of the fitting procedure, even though the

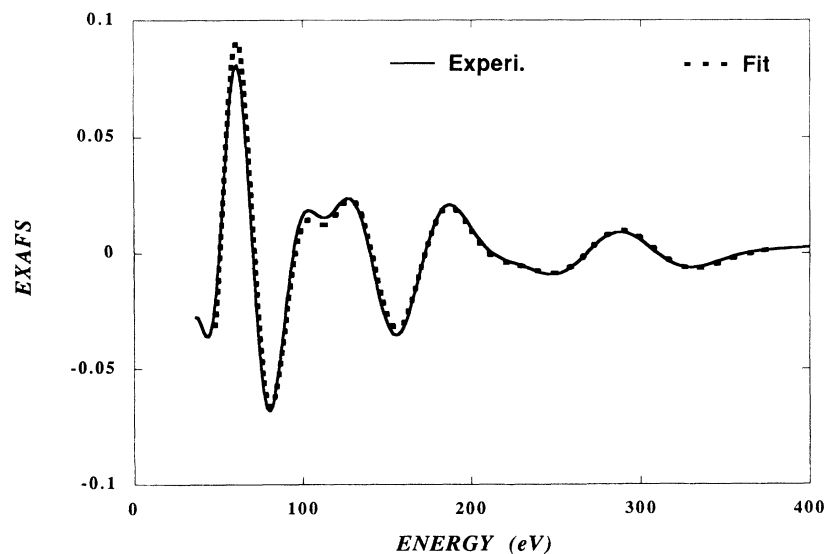

FIG. 6. Fit of the Fourier-filtered two first peaks for the laser-annealed 3×10^{16}-As/cm^2 sample. The absorption spectrum was measured by fluorescence detection.

real error bar is probably lower, since the results presented here are mean values of results obtained on several spectra measured during different experiments. Concerning the first-neighbors shell, the errors on the number of coordination are of the order of 10%, and 0.01–0.02 Å on the distance (depending on the spectra) and 1.2×10^{-3} on the Debye-Waller factor.

It should also be noted that the analysis of the second-neighbors shell requires much more care than the first one. This is due to the fact that this shell contains As and Si atoms at about the same distance to the central atom, as will be seen below. The number of highly correlated parameters required to describe the As and Si contributions was then too large to obtain good accuracy on quantitative values using least-square fitting in k space. Therefore, in the case of this second-neighbors shell, we have made some physical realistic hypothesis in order to reduce the number of free parameters. The total number of atoms, As and Si, was then fixed equal to 12 and the distance from the As central atom of the second-neighbor Si atoms was fixed at 3.81 Å. This distance was found in the BD crystal in which we assumed that no As atoms are present in the second shell due to the important dilution. In order to obtain the error bar on the number of As atoms present in this second-neighbors shell we then plotted the fitting-index contours, varying the number of As atoms in the shell and their distance from the As central atom or the Debye-Waller factor (see below). The error bars were estimated from the contour corresponding to the parameter FI equal to 1, as in the case of the first neighbors.

It is also worth noting that there exists a significant phase shift between the As and Si backscattered phases. Therefore, the presence of As and Si atoms in the same shell should lead to a decrease of the amplitude of the EXAFS signal, depending on the distances between these atoms and the central atom. This could lead to a decrease of the magnitude of the FT without a decrease of the total number of atoms.[25]

In order to compare the EXAFS amplitude obtained by TEY and fluorescence detection in the two different synchrotron centers, the angular divergence of each beamline for the experimental conditions described above was estimated, taking into account the divergence due to the monochromator and to the entrance slits. The energy resolution was described by a Gaussian distribution whose standard deviation is equal to $E\,\mathrm{cotg}(\theta_{hkl})\delta\theta$, where θ_{hkl} is the Bragg angle and $\delta\theta$ the angular divergence. We obtained 4.3 eV for EXAFS 1 at LURE and 1.2 eV for station 9.2 at Daresbury. Therefore, the theoretical phases used to analyze spectra taken in TEY mode were corrected using the EXAFS spectrum of the BD crystal previously convoluted by a Gaussian of standard deviation equal to 4.1 eV [e.g., $(4.3^2-1.2^2)^{1/2}$]. For the samples studied in TEY and fluorescence, the results found for the number of Si nearest neighbors are equal within 10%. In summary, we assumed the phase and amplitude transferability between TEY and fluorescence detection if the energy resolution is properly taken into account.

D. Model compounds

Several model compounds were studied in order to correct the theoretical phases: for the As-Si pairs crystalline SiAs and the BD crystal were used while, for the As-As pairs, amorphous As was chosen for the first neighbors and crystalline GaAs for the next-nearest neighbors.

For amorphous arsenic, the As-As distance was fitted with theoretical phase shifts. The As environment obtained is three As atoms at 2.48 Å, in agreement with the one given by Greaves, Elliott, and Davis.[26]

Since the SiAs crystal is monoclinic[19] a correction due to the linear polarization of the beam was made. The formula giving the effective number of nearest neighbors seen by EXAFS is $N^*=3\langle\cos^2\theta\rangle$, where θ is the angle between the polarization direction of the beam and the bond between the central atom and one of its neighbor. The average $\langle\cos^2\theta\rangle$ indicates a mean value over all the neighbors of the shell. In Fig. 7 we report the atomic distribution around an As atom in SiAs and the different contributions of each neighbor atom to the EXAFS sig-

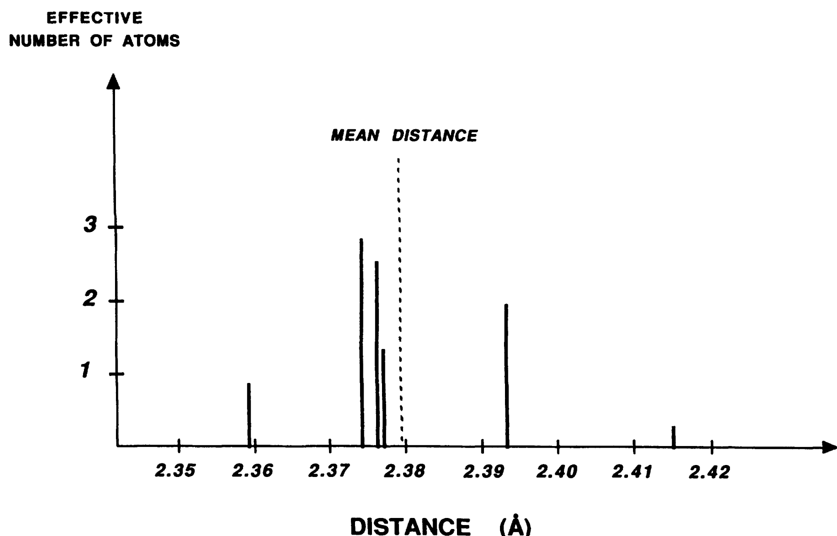

FIG. 7. Distribution of the Si atom distances around an As atom in crystalline SiAs [from Wadsten (Ref. 19)]. Three different As crystallographic sites, each with three Si nearest neighbors, were taken into account. The vertical scale represents an effective number of atoms as seen by EXAFS. Each atomic bond was corrected by a term $\langle\cos^2\theta\rangle$ in order to take into account the x-ray polarization of the beam.

TABLE II. Coordination number (N_{Si}) and distance ($d_{Si\text{-}Si}$, $d_{As\text{-}Si}$) of our different As-Si model compounds, together with the corresponding Debye-Waller factor σ^2. The values in parentheses were obtained from the experiment.

Samples	First shell N_{Si}	First shell $d_{Si\text{-}Si}$ (Å)	First shell σ^2 (10^{-3} Å^2)	Second shell N_{Si}	Second shell $d_{Si\text{-}Si}$ (Å)	Third shell N_{Si}	Third shell $d_{Si\text{-}Si}$ (Å)
Pure Si crystal[a]	4	2.35		12	3.84	12	4.50
	N_{Si}	$d_{As\text{-}Si}$ (Å)	σ^2 (10^{-3} Å^2)	N_{Si}	$d_{As\text{-}Si}$ (Å)	N_{Si}	$d_{As\text{-}Si}$ (Å)
SiAs crystal	3.3[b]	2.38[c]	(3.5[d])				
Bulk-doped crystal[d]	(4.0)	(2.41) (±0.01)	(2.5)	(12)	(3.81) (±0.02)	(12)	(4.48)

[a]From x-ray diffraction.
[b]Effective coordination number as obtained after the correction due to the linear polarization of the beam.
[c]From Wadsten (Ref. 19).
[d]Results obtained from a fit of the EXAFS spectrum with theoretical phase shifts.

nal according to the term $\langle \cos^2\theta \rangle$. Adding all these contributions leads to an effective number of first neighbors in crystalline SiAs of 3.3 atoms, instead of 3, at a mean distance of 2.38 Å (see Fig. 7).

It is important to note that the crystallographic structures of the two model compounds, SiAs and the BD Si crystal, are very different. Indeed, the crystalline SiAs is monoclinic and has a layered structure[19] leading to an asymmetric atomic distribution around an As atom. Consequently, the Debye-Waller factor, i.e., the mean-square width of the Gaussian distribution of distances, is probably strongly anisotropic. This atomic distribution is even more asymmetric if one takes into account the effective number of atoms seen by EXAFS. On the other hand the bulk-doped crystal is diamond cubic and the As atoms are assumed to be in substitutional positions, with four Si nearest neighbors, due to the very low concentration of As. Therefore, the atomic distribution around the As atoms is expected to be symmetric and narrow. Table II shows the environment of As atoms in our model compounds and the results obtained for the BD crystal as described above.

Concerning the choice of the reference samples, we have compared the results obtained using the SiAs and the BD crystals to correct the theoretical phases. The values of the As-Si distances always appear to be the same. As such, one could argue that both the BD and the SiAs samples could be equally well employed as a reference. However, this is not true, mainly because the values of the As coordination number are somewhat different. Namely, significant differences appear in the laser-annealed samples. In these samples, where arsenic is known to be in substitutional position, according to the RBS results[3,7,27] and electrical measurements,[1] the values of the As coordination, obtained with the SiAs crystal as a reference, are physically too high, e.g., about 5 instead of 4. On the contrary, the use of the BD crystal as a reference gives the expected As coordination (see Table III). As shown in Fig. 8, the FT's of the laser-annealed samples closely resemble that of the BD crystal: the

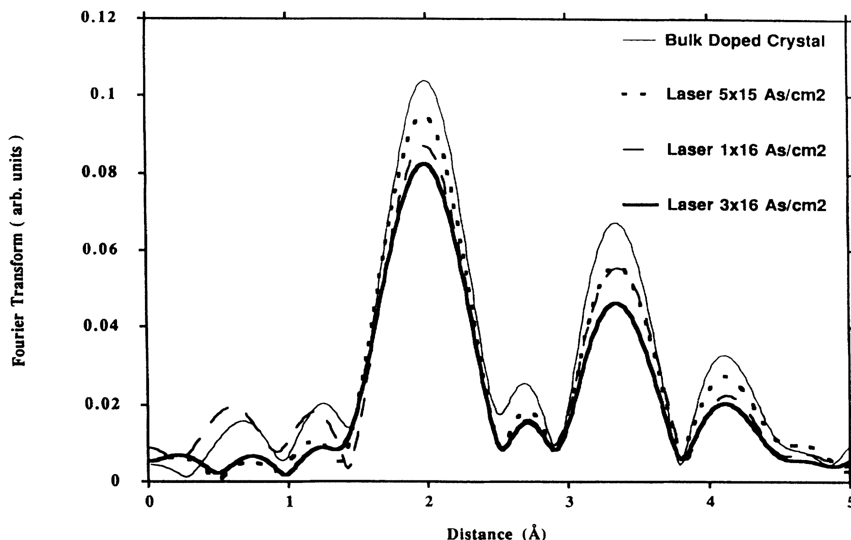

FIG. 8. Comparison of the moduli of the FT's of the EXAFS spectra of the BD sample and the laser-annealed samples for the three implanted doses studied (5×10^{15} As/cm^2, 1×10^{16}, and 3×10^{16} As/cm^2). The EXAFS spectra were obtained by fluorescence detection.

TABLE III. EXAFS results of the first shell of neighbors around an As atom. For each sample, the mean values reported here were estimated from the results obtained on the samples studied several times or by different detection modes. The error bars were obtained by doubling the residual at the minimum.

Dose As^+/cm^2	Annealing type	N_{Si}	$d_{As\text{-}Si}$ (Å)	σ^2 (10^{-3} Å^2)
5×10^{15}	Implanted	3.3±11%	2.38±0.015	5
	laser	4.1	2.41	3.5
	650 °C	3.9	2.39	4.5
	900 °C	3.9	2.40	4.5
1×10^{16}	Laser	3.9	2.41	4
3×10^{16}	Implanted	2.9±10%	2.38±0.01	4.5
	laser	4.2	2.40	4.3
	350 °C 40 min	3.4	2.40	3.3
	350 °C 80 min	3.2	2.39	4.7
	350 °C 640 min	3.2	2.38	2.8
	450 °C	2.7	2.36±0.02	2.7
	550 °C	2.2	2.37	2
	650 °C	3.2	2.37	3
	750 °C	3	2.36	2.3
	850 °C	3.4	2.38	4
	900 °C	3.1	2.37	2
	1000 °C	3.6	2.36	2
5×10^{16}	Implanted	2.8	2.37±0.01	3
	laser	3.9	2.41	4.7
	450 °C	2.9	2.37±0.02	4
	650 °C	2.7	2.37	1
	750 °C	2.7	2.35	2
	850 °C	3.6	2.38	4.5
	900 °C	3.1	2.35	3
	1000 °C	3.7	2.37	4.5

peaks corresponding to the three nearest-neighbors shells occur at the same distance but the amplitude of all the peaks is lower. This strongly suggests that the As atoms have the same short-range environment as in the BD crystal but with a more important static disorder in the distribution distances. In the case of the SiAs crystal, the discrepancy observed in the number of nearest neighbors is then due to its different crystallographic structure with respect to the laser-annealed samples, which leads to a nontransferability of the backscattered amplitude between these samples. Instead, in the samples further annealed between 350 and 1000 °C, when the deactivation process is significant, the As coordination numbers obtained with the two model compounds are very close, namely about three Si neighbors at a distance of 2.38 Å. In this case, the amplitude transferability between these samples and the SiAs crystal is correct, as the local environment is the same. In summary, the use of the BD crystal as a reference always gives physically correct results, unlike the SiAs crystal. Therefore, all the results presented here were obtained with theoretical phase shifts corrected with the BD crystal.

III. RESULTS

The results and the error bars for the *first-neighbors shell,* obtained as described above, are reported in Table III. Within this first shell one notices that, for all the samples, no significant As contribution was found, at least within the accuracy of the measurements. Canova *et al.*,[28] in polycrystalline Si-doped As, and Erbil *et al.*[27] in crystalline Si, came to the same conclusion. This trend strongly suggests that the local structure with As-As as first neighbors is not favored.

A. Dilute specimen

Since the concentration of As atoms (0.04%) in the BD sample is low enough to ensure that all the As atoms are in substitutional position in the Si matrix, it can be used to extract the exact local deformation due to the size difference between As and Si. The results obtained with theoretical phases, without any linear corrections, using EXCURV88 (see Table II), show the nearest-neighbor As-Si distance results to be equal to 2.41±0.01 Å, in agreement with the EXAFS measurements of Erbil *et al.*[27] obtained on Si specimens doped with 0.1, 0.7, and 7 a.t. % As. This value also agrees with those obtained from different theoretical models: for example, Bechstedt and Harrison,[29] using the bond-orbital approximation, found a value of 2.42 Å. Concerning the second-neighbors shell, the distance between the Si atoms and the As central atom was found to be equal to 3.81±0.02

Å. This value is slightly lower than the crystallographic value of 3.84 Å in pure silicon.

B. As-implanted specimens

After implantation, and before any annealing, the samples are amorphous and, with the EXAFS technique, only the first-neighbors shell is visible. No significant variation of the As environment was observed with the dopant dose. Indeed, for the three doses studied, 5×10^{15} As/cm^2, 3×10^{16}, and 5×10^{16} As/cm^2, the same result was obtained: 3 ± 0.3 Si atoms at 2.38 ± 0.01 Å. This local environment around the As atoms is the same as in crystalline SiAs and is in agreement with the one found by Knights, Hayes, and Mikkelsen[30] in *a*-Si:H. This coordination of three was also found by Greaves *et al.*[31] in *a*-Si-H and amorphized silicon with a slightly lower distance of 2.36 ± 0.01 Å for the inactive sites.

C. Laser-annealed specimens

In the initial metastable state obtained after crystalline regrowth by laser annealing, the As atoms are in a substitutional tetracoordinated site, although in a highly supersaturated state. Each As atom is then surrounded by four Si atoms at a distance of 2.41 ± 0.01 Å, in agreement with Erbil *et al.*[27] This value is much larger than in pure crystalline silicon (2.35 Å) and reflects the local dilatation due to the larger atomic radius of As. The same distance of 2.41 Å was found in the case of the dilute specimen. As in the case of the as-implanted specimens, the environment around the As atoms does not depend on the implanted dose between 5×10^{15} and 5×10^{16} As/cm^2. It is also worthwhile to note that the Debye-Waller factors are significantly high. This point is consistent with the previous remark concerning the important local static disorder of the first neighbors. This disorder is probably caused by the presence of As atoms in the near neighborhood, since the magnitude of the different peaks of the FT's decreases as the implanted dose increases (Fig. 8).

D. High-dose-annealed specimens (3×10^{16} and 5×10^{16} As/cm^2)

During the furnace annealing, the metastable solid solution tends to return to its equilibrium solubility value and several drastic changes occur on the nearest neighbors of the As atoms for the two highest doses studied, 3×10^{16} and 5×10^{16} As/cm^2.

(i) The coordination number decreases from 4.2 ± 0.4 to 3.2 ± 0.3 during the isothermal annealing at 350 °C. For the first time, it is clearly shown that this decrease is correlated to the electrical deactivation that occurs at the same temperature [Table I and Fig. 9(a)]. Simultaneously, the As-Si distance decreases slightly.

(ii) The As-Si distance of the first neighbors becomes equal to 2.37 ± 0.02 Å when the deactivation is complete. At the same time, the coordination number is reduced from 4 to 3 atoms, approximately, for an annealing temperature below 750 °C, as shown in Fig. 9(b). On the contrary, when the annealing temperature increases from

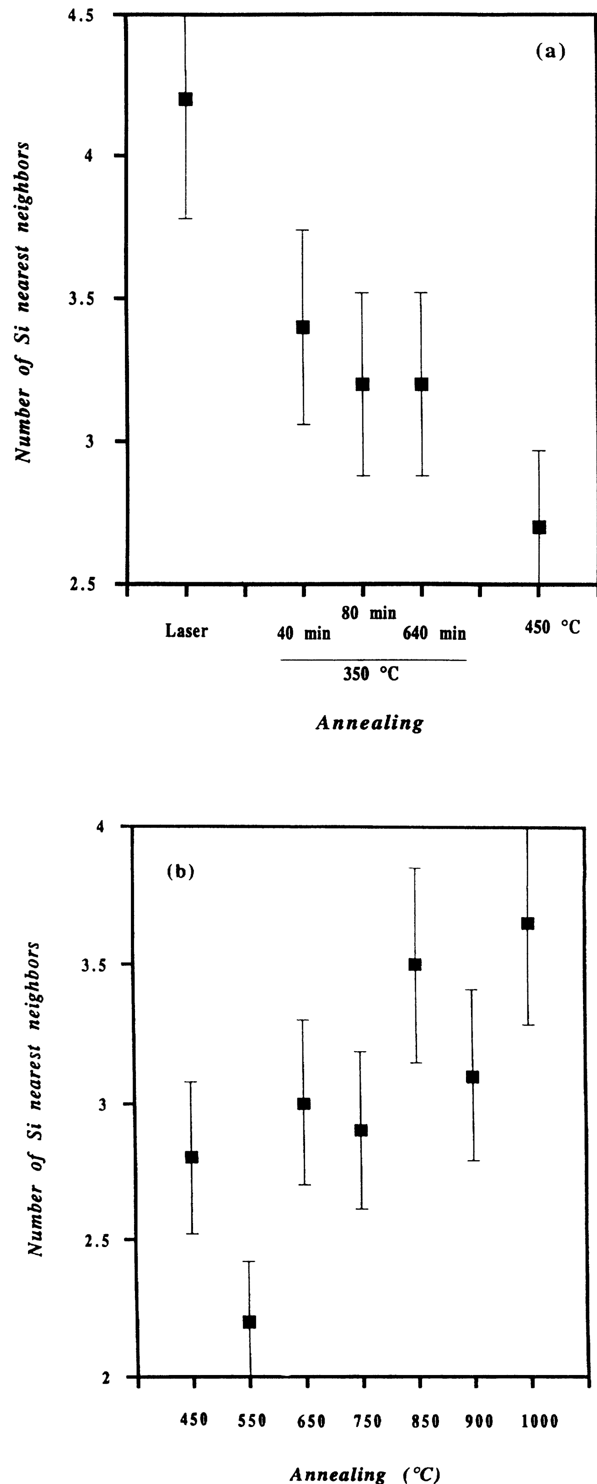

FIG. 9. Number of Si nearest neighbors around an As atom (the mean values reported were estimated from the results obtained on the samples studied several times or by different detection modes). (a) 3×10^{16}-As/cm^2 samples isothermally annealed at 350 °C plus the laser-annealed one and the equilibrium state at 450 °C. (b) Equilibrium state of the deactivation process for an annealing temperature between 450 and 1000 °C. The number of atoms shown are mean values of the results obtained for the two implanted doses: 3×10^{16} and 5×10^{16} As/cm^2.

TABLE IV. EXAFS results of the second shell of neighbors around an As atom. The number of atoms is deduced using the fitting-index contours similar to the one in Fig. 10.

Dose	Annealing type	Number of As second-nearest neighbors
3×10^{16} ions/cm^2	Laser	1 ± 1
	350 °C 80 min	3 ± 3
	450 °C	5 ± 3
	550 °C	6 ± 4

750 °C up to 1000 °C, it appears, from Fig. 9(b), that the number of Si nearest neighbors increases slightly up to 3.7 ± 0.4 atoms.

Concerning the *second-nearest-neighbors shell*, the Fourier transforms indicate directly that the second peak decreases in magnitude with the deactivation of the As atoms (Fig. 5). This trend also appears clearly during the isothermal annealing at 350 °C (Fig. 3). This decrease of the peak magnitude can be explained by an increase of the number of As atoms or by an increase of the Debye-Waller factor, i.e., an increase of the static disorder. In order to distinguish between these two hypotheses, a quantitative analysis is necessary. Simultaneous presence of As and Si atoms is assumed and fitting-index contours corresponding to a variation of (i) the atom number, (ii) the Debye-Waller factor, or (iii) the distance to the central atom (Fig. 10), are plotted. Results at 3×10^{16} As/cm^2 are summarized in Table IV. One notes a significant increase in the number of As second-nearest neighbors at 450–550 °C annealing temperature.

The changes in the second-neighbors peak for annealing temperatures higher than 550 °C are too small (see the second peaks in Fig. 5) to deduce any further evolution of the number of As atoms.

E. The 5×10^{15} As/cm^2-implanted dose

The case of the lowest implanted dose (5×10^{15} As/cm^2) seems to imply, at first view, a different mechanism. The experimental results shows only a slight decrease of the number of Si nearest neighbors and a more significant decrease of the As-Si distance under thermal annealing (Table III). However, at such a low dose, not only the accuracy in the determination of the nearest-neighbors number deteriorates, but 50% of the As atoms are also in a substitutional position at 650 °C as well as at 900 °C (see Table I). As a consequence, the EXAFS technique probes a mixture of two configurations in approximately the same number. The apparent nearest-neighbor number should be the average of the substitutional position number (equal to 4) and of the position number proposed for the deactivated states (equal, respectively, to 3.2 at 650 °C and 3.1 at 900 °C), thus giving approximately a value of 3.6. Similarly, the average Si-As distance should be close to 2.39 Å. These figures are in the error margin of the experimental results measured at 5×10^{15} As/cm^2 and the proposed model is still compatible with the low implanted dose.

IV. DISCUSSION

A. Low-temperature annealing ($350 < T < 650$ °C)

The usual assumptions made in order to explain the As deactivation are the formation of inactive clusters or precipitates. By transmission electron microscopy, precipitates have only been observed for high-temperature annealing ($T > 850$ °C).[1,2] Therefore, the electrical deactivation observed at lower annealing temperatures can only be explained by the formation of inactive clusters that could be metastable and/or act as embryos for the precipitates at higher temperature. The exact shape and nature of these embryos are still unclear except for the first shell

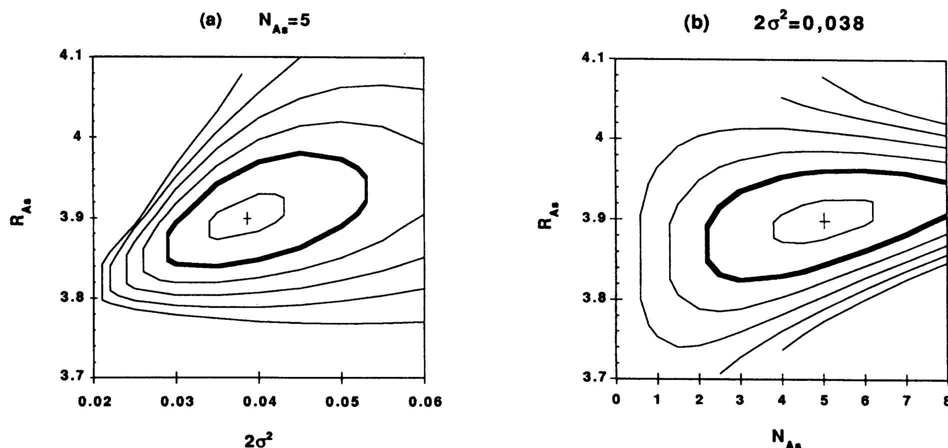

FIG. 10. Fitting-index contours of the second-neighbors shell obtained on the 3×10^{16}-As/cm^2 samples annealed at 450 °C, whose TF is presented in Fig. 3, by varying the (a) Debye-Waller factor or (b) the number of As atoms in the shell. N_{As} is the number of As atoms in the shell, R_{As} their distance to the central As atom, and σ^2 the Debye-Waller factor of the shell. The heavy line represents the contour corresponding to FI equal to 1, which was used to estimate the error bar (see text).

around the As atoms. The decrease of one atom (from 4 to 3) in the number of Si nearest neighbors as soon as the deactivation proceeds clearly indicates that one vacancy is involved in these clusters. The main local structures involving a vacancy that have been proposed are As_4V studied by Pandey *et al.*[13] and As_2V, which we recently suggested.[1] In the two cases, the short-range structure around an As atom becomes the same as in crystalline SiAs, i.e., three Si atoms at 2.38 Å. The present work extends the previous studies to lower annealing temperatures. As a consequence, it is now clearly established that the changes in the coordination number and the As-Si distance occur simultaneously with the electrical deactivation of the As atoms. Therefore, this structural change can now be attributed to the deactivation phenomenon. In fact, As atoms have a natural coordination of three, as in amorphous and crystalline arsenic, but the laser annealing is so fast that As atoms are "frozen" in substitutional position in the Si matrix with a coordination of four. On the contrary, during a long annealing, it is possible to create a vacancy by emission of a Si interstitial in order to recover the natural coordination of three.

The second-shell changes observed after the As deactivation, are also significant and indicate clearly an agglomeration of As atoms in second-neighbors position. In the temperature range of 450–550 °C, our quantitative interpretation of this shell has led to a number of 6 ± 4 As atoms, in agreement with the results obtained by Pandey *et al.*[13] for a heavier implanted dose (6×10^{16} As/cm^2).

In the temperature range 350–650 °C, the electrical deactivation was then clearly identified to be due to the formation of complexes As_mV consisting of up to 7 ± 4 As atoms around a vacancy (including the central As atom). The important error bar existing on the m determination does not allow us to conclude whether the structure of these clusters evolves continuously with the annealing temperature or with the amount of deactivated atoms, for example, from As_2V into As_6V. However, m is already greater than 2 at 450 and 550 °C and there is a tendency for m to increase with the annealing temperature. Therefore, the As_2V structure, if it exists, is a transient structure and is limited to the very first annealing steps.

B. High-temperature annealing ($750 < T < 1000$ °C)

The detailed measurements made between 450 and 1000 °C [Fig. 9(b)] show that the As_mV complexes clearly seen between 450 and 650 °C are not the final configuration. Indeed, it has been observed that *the number of Si first neighbors* tends back to four atoms at high temperature. This observation cannot be explained by the As redissolution in solid solution, the As content being much larger than the solubility limit at 1000 °C. On the contrary, it is probably connected to the precipitates observed by microscopy in this temperature range. Therefore, one can suppose that the As_mV clusters existing at lower temperature can act as embryos for the formation of these precipitates. The sphalerite SiAs, which has been proposed after the electron-microscope observation of precipitates above 850 °C,[2] is, therefore, compatible with our measured values since, in this structure, the As atoms are tetracoordinated. At these temperatures, the As atoms could then be found with three different local atomic structures at the equilibrium state: (i) electrically active in substitutional position, (ii) in an inactive cluster As_mV, and (iii) in a precipitate, as recently suggested by Parisini *et al.*[32]

V. CONCLUSION

Using two different techniques to measure the EXAFS signal (total electron yield and fluorescence detection) on As heavily implanted crystalline samples, we were able to study a large range of implanted doses, from 5×10^{15} As/cm^2 to 5×10^{16} As/cm^2. The local structure around an As atom during the different stages of the As deactivation after a laser and a subsequent thermal annealing, in the range 350–1000 °C is described. It is shown that the agglomeration process is already active during the As deactivation. Moreover, from the careful study of the two first shells of As neighbors, we propose a model in which, for the 3×10^{16} As/cm^2 implanted dose and for annealing temperatures below 750 °C, the electrical deactivation is due to the agglomeration of 7 ± 4 As atoms around one vacancy, leading to the formation of inactive clusters As_mV and to a local structure resembling the crystalline SiAs one. At higher annealing temperatures, above 750 °C, these clusters could act as embryos for the formation of SiAs precipitates with the sphalerite structure, previously observed by electron microscopy.

ACKNOWLEDGMENTS

The authors are indebted to Professor G. N. Greaves (Daresbury) for fruitful discussions and assistance during the experiments. The assistance of M. Ladouceur at LURE, K. J. Roberts, and R. Billsborrow at Synchrotron Radiation Center, Daresbury Laboratory was also greatly appreciated. Thanks are also due to G. Queirolo, E. Gabilli, P. Negrini, and L. Correra for the implantation, laser, and thermal annealing of the silicon wafers.

[1]A. Parisini, A. Bourret, A. Armigliato, M. Servidori, S. Solmi, R. Fabbri, J. R. Regnard, and J. L. Allain, J. Appl. Phys. **67**, 2320 (1990).

[2]A. Armigliato, D. Nobili, S. Solmi, A. Bourret, and P. Werner, J. Electrochem. Soc. **133**, 2563 (1986).

[3]A. Erbil, G. S. Cargill III, and R. F. Boehme, in *Advanced Photon and Particle Techniques for the Characterization of Defects in Solids*, edited by J. B. Roberts, R. W. Carpenter, and M. C. Wittels, MRS Symposia Proceedings No. 41 (Materials Research Society, Pittsburgh, 1985), p. 275.

[4]A. Lietoila, J. F. Gibbons, and T. W. Sigmon, Appl. Phys. Lett. **36**, 765 (1980).

[5]D. Nobili, A. Carabelas, G. Celotti, and S. Solmi, J. Electrochem. Soc. **132**, 922 (1983).

[6]R. Angeluci, G. Celotti, D. Nobili, and S. Solmi, J. Electrochem. Soc. **132**, 2729 (1985).

[7]W. K. Chu and B. J. Masters, in *Laser-Solid Interactions and Laser Processing—1978* (Materials Research Society, Boston), Proceedings of The Symposium on Laser-Solid Interactions and Laser Processing, edited by S. D. Ferris, H. J. Learny, and J. M. Poate, AIP Conf. Proc. No. 50 (AIP, New York, 1978), p. 305.

[8]S. J. Pennycock, R J. Culbertson, and J. Narayan, J. Mat. Res. **1**, 476 (1986).

[9]N. R. Wu, D. K. Sadana, and J. Washburn, Appl. Phys. Lett. **44**, 782 (1984).

[10]A. Parisini, A. Bourret, and A. Armigliato, in *Microscopy of Semiconducting Materials,* Proceedings of the Institute of Physics Conference at Oxford University, edited by A. G. Cullis and P. D Augustus, IOP Conf. Proc. No. 87 (Institute of Physics and Physical Society, London, 1987), p. 491.

[11]A. Lietoila, J. F. Gibbons, T. J. Magee, J. Peng, and J. D. Hong, Appl. Phys. Lett. **35**, 532 (1979).

[12]R. B. Fair and G. R. Weber, J. Appl. Phys. **44**, 273 (1973).

[13]K. C. Pandey, A. Erbil, G. S. Cargill III, R. F. Boehme, and D. Vanderbilt, Phys. Rev. Lett. **61**, 1282 (1982).

[14]E. Guerrero, H. Potzl, R. Tielert, M. Grasserbauer, and G. Stingeder, J. Electrochem. Soc. **129**, 1827 (1982).

[15]R. O. Schwenker, E. S. Pan, and R. F. Lever, J. Appl. Phys. **42**, 3195 (1971).

[16]M. Y. Tsai, F. F. Morehead, J. E. E. Baglin, and A. E. Michel, J. Appl. Phys. **51**, 3230 (1980).

[17]V. I. Fistul, *Heavily Doped Semiconductors* (Plenum, New York, 1969).

[18]P. M. Fahey, P. B. Griffin, and J. D. Plummer, Rev. Mod. Phys. **61**, 289 (1989).

[19]T. Wadsten, Acta Chem. Scand. **19**, 1232 (1965).

[20]A. Armigliato and A. Parisini, J. Mater. Res. **6**, 1701 (1991).

[21]G. Tourillon, E. Dartyge, A. Fontaine, M. Lemonnier, and F. Bartol, Phys. Lett. A **121**, 251 (1987).

[22]W. T. Elam, J. P. Kirkland, R. A. Neiser, and P. D. Wolf, Phys. Rev. B **38**, 26 (1988).

[23]J. Stöhr, C. Noguera, and T. Kendelewicz, Phys. Rev. B **30**, 5571 (1984).

[24]S. J. Gurman, N. Binsted, and I. Ross, Solid State Phys. **17**, 143 (1986).

[25]J. Mimault, A. Fontaine, P. Lagarde, D. Raoux, A. Sadoc, and D. Spanjaard, J. Phys. F **11**, 1311 (1981).

[26]G. N. Greaves, S. R. Elliott, and E. A. Davis, Adv. Phys. **28**, 49 (1979).

[27]A. Erbil, W. Weber, G. S. Cargill III, and R. F. Boehme, Phys. Rev. B **34**, 1392 (1986).

[28]E. Canova, Y. H. Kao, T. Marshall, and E. Arnold, Phys. Rev. B **39**, 3131 (1989).

[29]F. Bechstedt and U. A. Harrison, Phys. Rev. B **39**, 5041 (1989).

[30]J. C. Knights, T. M. Hayes, and J. C. Mikkelsen, Jr., Phys. Rev. Lett. **39**, 712 (1977).

[31]G. N. Greaves, A. J. Dent, S. Kalbitzer, S. Pizzini, and G. Müller, Phys. Rev. B **45**, 6517 (1992).

[32]A. Parisini, D. Nobili, A. Armigliato, M. Derdour, L. Moro, and S. Solmi, Appl. Phys. A **54**, 221 (1992).